

# Ir(III) Phosphors Modified with Fluorine Atoms in Pyridine-1,2,4-triazolyl Ligands for Efficient OLEDs Possessing Low-Efficiency Roll-off

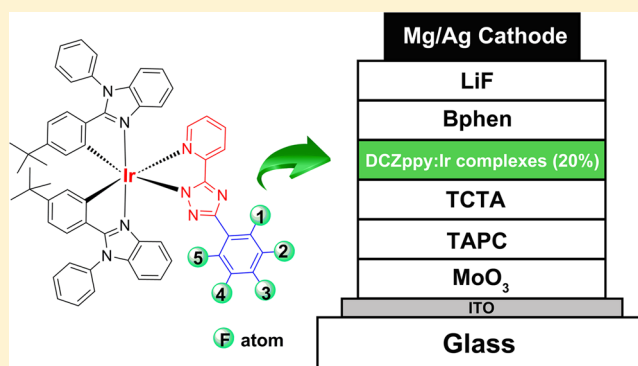
Hui-Ting Mao,<sup>†</sup> Chun-Xiu Zang,<sup>‡</sup> Li-Li Wen,<sup>†</sup> Guo-Gang Shan,<sup>\*,†</sup> Hai-Zhu Sun,<sup>†</sup> Wen-Fa Xie,<sup>\*,‡</sup> and Zhong-Min Su<sup>\*,†</sup>

<sup>†</sup>Institute of Functional Material Chemistry and National & Local United Engineering Lab for Power Battery, Faculty of Chemistry, Northeast Normal University, Changchun 130024, People's Republic of China

<sup>‡</sup>State Key Laboratory on Integrated Optoelectronics, College of Electronic Science and Engineering, Jilin University, Changchun, Jilin 130012, People's Republic of China

## Supporting Information

**ABSTRACT:** Five neutral heteroleptic Ir(III) complexes 1–5 using the same cyclometalated ligand and different pyridine-1,2,4-triazolyl derivatives as ancillary ligands with fluorine substituents attached, were rationally designed and prepared. Their photophysical, electrochemical, and thermal properties were studied, and theoretical calculations were performed to understand the emission behaviors as well. Introducing fluorine atoms has little effect on the photophysical and thermal properties, but the performances of the resulting devices can be fine-tuned. Among them, a heavy doping level device employing a phosphor with five fluorine atoms delivers superior device efficiencies with  $\eta_c = 32.6 \text{ cd A}^{-1}$  and  $\eta_p = 27.6 \text{ lm W}^{-1}$ , respectively, which is higher than those of other counterparts. Importantly, such a device exhibits almost negligible roll-off in luminance efficiency. Despite nondoped devices achieving good EL performance, more fluorine atoms lead to a relatively higher efficiency roll-off. The results suggest that rational incorporation of fluorine atoms into the ancillary ligands can significantly improve the performance of devices with features of high efficiency and small roll-off.



## 1. INTRODUCTION

Organic light-emitting diodes (OLEDs) have drawn extensive attention in recent years owing to their foreseeable effect in both flat-panel displays and solid-state lighting.<sup>1</sup> Among the related reports, phosphorescent OLEDs have continued to attract significant research interest because of their high intrinsic efficiency. Phosphorescent heavy-metal organic complexes give an advantage over their fluorescent counterparts, in which both the electrogenerated singlet and triplet excitons forming on charge recombination can be harvested and decay radiatively, theoretically leading to 100% internal quantum efficiency.<sup>1,2</sup> Among these, Ir(III) complexes are of particular importance as a series of outstanding phosphorescent materials due to appropriate exciton lifetimes, high luminescence quantum yields, and facile color tuning through control of the ligand structure.<sup>3</sup> Nevertheless, a number of challenges remain; in particular, quenching of the luminescence caused by intermolecular interactions and typically poor carrier mobility result in substantial deficits, which prevent them from being used in an undiluted form as the emission layer (EML).<sup>4</sup> Therefore, most high-performance devices based on Ir(III) phosphors have to disperse into a suitable host to improve the

energy transfer and avoid self-quenching.<sup>4b,5</sup> However, efficacious doping often requires careful control of the doping concentration, resulting in a restriction on their reproducibility in mass production, which needs high consistency for production quality.<sup>5c,6</sup> In addition, the potential phase separation occurring in blended systems usually leads to poor energy transfer and device degradation over time.<sup>4b,5c,7</sup>

Recently, significant efforts have been made to develop high-performance Ir(III)-based OLEDs with a nondoped and/or heavy doping level emitting layer. Nondoped OLEDs have the benefit of being able to overcome the problems mentioned above, as the EML is only composed of a single Ir(III) complex; thus, the device performance apparently depends on material performance.<sup>4b,8</sup> Additionally, heavy doping level OLEDs could also make a sophisticated control of the doping process unnecessary, which is greatly beneficial for improving the product yield of commercial mass production in the future.<sup>8,9</sup> In 2002, Chen et al. designed and synthesized a new complex based on 2,3-(bis-*N,N*-1-naphthylphenylamino)-*N*-

Received: September 24, 2016

ethylmaleimide, giving a red emission nondoped device with state of the art efficiency and luminance.<sup>10</sup> Peng et al. reported the nondoped phosphorescent Ir(III) complex (ppy)<sub>2</sub>Ir(dipig), which realized a respectable external quantum efficiency (EQE) up to 18%, accompanied by outstanding power efficiency as high as 70 lm W<sup>-1</sup>.<sup>6c</sup> Our group and others have demonstrated a series of excellent Ir(III) complexes containing 1,2-diphenyl-*H*-benzoimidazole (Hpbil) for the purpose of understanding the relationship between molecular structures and device performances, in which Hpbil-type ligands can be easily synthesized and modified in relatively high yield.<sup>11</sup> The fabricated OLEDs not only exhibited promising performance but also displayed little efficiency roll-off at high brightness.<sup>3f</sup> Despite the achieved advances, constructing Ir(III) complexes capable of giving high-performance OLEDs with nondoped and/or highly doped features still remains a significant challenge to date.

Recently, phosphorescent emitters with the incorporation of the simple electron-withdrawing character of fluorine atoms in cyclometalated ligands were employed to tune the emission colors to a high-energy region. The corresponding reports indicated that fluorinated substituents in the cyclometalating ligand may impose severe limitation on the long-term device stability.<sup>12</sup> However, such a design strategy can enhance the photoluminescence (PL) efficiency of phosphors due to the lower vibrational frequency of C–F bonds.<sup>13</sup> Fluorine atoms readily form strong inter-/intramolecular interactions with the neighboring molecules, thereby controlling the solid-state packing and intrinsic characters. In addition, adding fluorine atoms indeed makes it possible to decorate with the ancillary ligands reasonably. Nevertheless, such a design strategy with the aim of tuning the properties of phosphorescent emitters to furnish highly efficient devices has not yet been well interpreted.

With this fundamental concern, we designed and synthesized a series of phosphorescent Ir(III) complexes **1–5** (Scheme 1) consisting of pyridine-1,2,4-triazolyl derivatives as ancillary ligands modified with electron-withdrawing fluorine atoms. The ancillary ligands L<sub>1</sub>–L<sub>5</sub> are 2-(3-(3,5-dimethylphenyl)-1*H*-1,2,4-triazol-5-yl)pyridine, 2-(3-phenyl-1*H*-1,2,4-triazol-5-yl)pyridine, 2-(3-(4-fluorophenyl)-1*H*-1,2,4-triazol-5-yl)pyridine, 2-(3-(3,5-difluorophenyl)-1*H*-1,2,4-triazol-5-yl)pyridine, and

2-(3-(perfluorophenyl)-1*H*-1,2,4-triazol-5-yl)pyridine, respectively. Two contributing factors of the ancillary ligand are as follows: (i) easy synthetic chemical accessibility and (ii) exceedingly large ππ\* energy gaps allowing the cyclometalated ligand to tune the final emission color.<sup>11b,14</sup> Thereby, it would be ideal to understand the influence of the fluorine substituents on the device performance while maintaining similar structures and the same emission colors. Complexes **1–5** exhibited strong emission at 498, 497, 495, 496, and 494 nm at room temperature, respectively. Both heavy doping level (20%) and nondoped devices employing **1–5** as emitting layers have been fabricated. Increasing the numbers of fluorine substituents only slightly affects the photophysical and thermal properties, but the device performance has been significantly enhanced. A heavy doping level (20%) device based on complex **5**, incorporating five fluorine substituents, reveals comparable efficiencies with η<sub>c</sub> = 32.6 cd A<sup>-1</sup> and η<sub>p</sub> = 27.6 lm W<sup>-1</sup>, respectively. It is worth noting that the fabricated devices show little roll-off in efficiency with increasing brightness.

## 2. EXPERIMENTAL SECTION

**2.1. General Information.** The reagents used in this work were commercially available. The solvents were purified by a conventional procedure and freshly distilled under argon before use. The <sup>1</sup>H NMR spectra were confirmed using a Bruker Avance 500 MHz instrument, in which CDCl<sub>3</sub> was used as the solvent and tetramethylsilane (TMS) as the internal reference. The mass spectra of the emitters were recorded on an electrospray ionization mass spectrometer (ESI-MS).

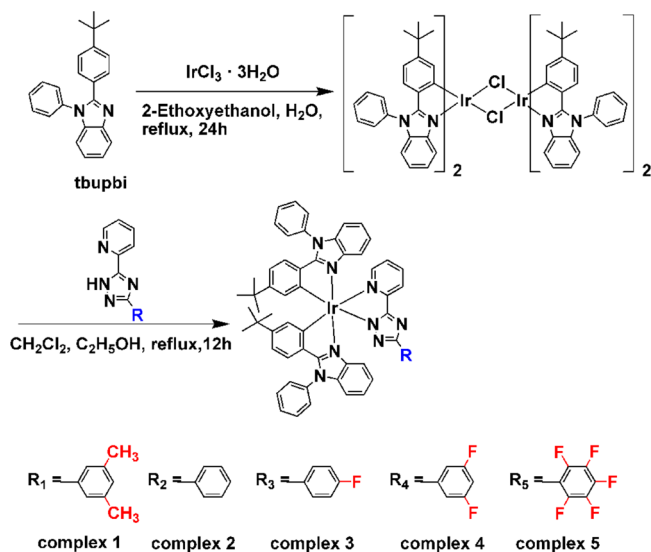
The absorption and photoluminescence spectra were observed with a Cary 500 UV–vis–NIR spectrophotometer and FL-4600 FL spectrophotometer, respectively. The thin films of **1–5** were prepared by spin-coating in CH<sub>2</sub>Cl<sub>2</sub> solution at a concentration at 20 mg mL<sup>-1</sup>. The excited-state lifetimes (τ) and photoluminescence quantum yields (Φ<sub>p</sub>) in solution from the samples were recorded on a spectrofluorimeter (Edinburgh FLS-920). The thermal gravimetric analysis (TGA) was carried out on a Perkin-Elmer TG-7 analyzer through heating the samples from 50 to 800 °C under a nitrogen atmosphere.

**2.2. Synthesis of Ligands Used in This Work.** The cyclometalated ligand 2-(4-*tert*-butylphenyl)-1-phenyl-1*H*-benzo[*d*]imidazole (tbupbi) and the ancillary ligands L<sub>1</sub>–L<sub>5</sub> (see Scheme S1 in the Supporting Information) were synthesized according to previous reports.<sup>12,15</sup>

**2.3. Synthesis of Complexes 1–5.** **2.3.1. Synthesis of Complex 1.** One equivalent of IrCl<sub>3</sub>·3H<sub>2</sub>O (0.35 g, 1 mmol) and 2.2 equiv of tbupbi (0.71 g, 2.20 mmol) were dissolved in 2-ethoxyethanol (30 mL) and water (10 mL), and the mixture was stirred under an argon atmosphere for 24 h. After it was cooled, the mixture was washed with water and ethanol and the formed precipitate was filtered, assumed to be a chloro-bridged dimer. Without further purification, [Ir-(tbupbi)<sub>2</sub>Cl]<sub>2</sub> (0.24 g, 0.16 mmol) and ligand L<sub>1</sub> (0.09 g, 0.40 mmol) were refluxed in a mixture of dichloromethane and ethanol for 12 h. After it was cooled to room temperature, the reaction mixture was extracted with CH<sub>2</sub>Cl<sub>2</sub> and then dried over anhydrous Na<sub>2</sub>SO<sub>4</sub>. The product was obtained by silica gel column chromatography with 1/20 (v/v) ethyl acetate/dichloromethane as eluent to give complex **1** (0.20 g) in a yield of 67%. <sup>1</sup>H NMR (500 MHz, CDCl<sub>3</sub>, δ [ppm]): 8.33 (d, *J* = 8.0 Hz, 1H), 7.82–7.87 (m, 4H), 7.57–7.68 (m, 8H), 7.37 (t, *J* = 8.5 Hz, 2H), 6.98–7.13 (m, 6H), 6.86–6.91 (m, 2H), 6.62–6.67 (m, 2H), 6.57–6.60 (m, 2H), 6.50–6.54 (m, 3H), 5.98 (d, *J* = 8.0 Hz, 1H), 2.33 (s, 6H), 0.93 (s, 9H), 0.92 (s, 9H). MS: calcd *m/z* 1092.4 for [M]<sup>+</sup> (C<sub>61</sub>H<sub>55</sub>IrN<sub>8</sub>), found *m/z* 1092.4. Anal. Calcd for C<sub>61</sub>H<sub>55</sub>IrN<sub>8</sub>: C, 67.07; H, 5.07; N, 10.26. Found: C, 66.98; H, 5.12; N, 10.32.

**2.3.2. Synthesis of Complex 2.** The product was obtained by silica gel column chromatography with a 1/20 (v/v) ethyl acetate/dichloromethane mixture as eluent to give complex **2** (0.20 g) in a yield of 69%. <sup>1</sup>H NMR (500 MHz, CDCl<sub>3</sub>, δ [ppm]): 8.32 (d, *J* = 8.5

Scheme 1. Synthesis of Ir(III) Complexes **1–5**



H<sub>z</sub>, 1H), 8.20 (d, *J* = 7.5 Hz, 2H), 7.81–7.88 (m, 2H), 7.55–7.70 (m, 8H), 7.36 (t, *J* = 7.5 Hz, 4H), 7.26 (s, 1H), 6.98–7.15 (m, 6H), 6.89 (t, *J* = 8.0 Hz, 1H), 6.63–6.67 (m, 2H), 6.60 (d, *J* = 8.5 Hz, 1H), 6.51–6.56 (m, 4H), 5.99 (d, *J* = 8.0 Hz, 1H), 0.92 (s, 9H), 0.92 (s, 9H). MS: calcd *m/z* 1064.4 for [M]<sup>+</sup> (C<sub>59</sub>H<sub>51</sub>IrN<sub>8</sub>), found *m/z* 1064.4. Anal. Calcd for C<sub>59</sub>H<sub>51</sub>IrN<sub>8</sub>: C, 66.58; H, 4.83; N, 10.53. Found: C, 66.65; H, 4.92; N, 10.60.

**2.3.3. Synthesis of Complex 3.** The product was obtained by silica gel column chromatography with 1/20 (v/v) ethyl acetate/dichloromethane and then 1/10 (v/v) ethyl acetate/dichloromethane as eluent to give complex 3 (0.22 g) in a yield of 73%. <sup>1</sup>H NMR (500 MHz, CDCl<sub>3</sub>, δ [ppm]): 8.30 (d, *J* = 7.5 Hz, 1H), 8.17 (s, 2H), 7.89 (d, *J* = 5.0 Hz, 1H), 7.83 (t, *J* = 7.5 Hz, 1H), 7.54–7.69 (m, 8H), 7.36 (t, *J* = 8.0 Hz, 2H), 6.98–7.15 (m, 8H), 6.89 (t, *J* = 8.0 Hz, 1H), 6.62–6.67 (m, 2H), 6.50–6.56 (m, 5H), 5.98 (d, *J* = 7.5 Hz, 1H), 0.92 (s, 9H), 0.92 (s, 9H). MS: calcd *m/z* 1082.4 for [M]<sup>+</sup> (C<sub>59</sub>H<sub>50</sub>FlrN<sub>8</sub>), found *m/z* 1082.4. Anal. Calcd for C<sub>59</sub>H<sub>50</sub>FlrN<sub>8</sub>: C, 65.47; H, 4.66; N, 10.35. Found: C, 65.41; H, 4.76; N, 10.43.

**2.3.4. Synthesis of Complex 4.** The product was obtained by silica gel column chromatography with 1/20 (v/v) ethyl acetate/dichloromethane and then 1/10 (v/v) ethyl acetate/dichloromethane as eluent to give complex 4 (0.21 g) in a yield of 70%. <sup>1</sup>H NMR (500 MHz, CDCl<sub>3</sub>, δ [ppm]): 8.30 (d, *J* = 8.0 Hz, 1H), 7.90 (d, *J* = 5.0 Hz, 1H), 7.84 (t, *J* = 7.5 Hz, 1H), 7.55–7.73 (m, 10H), 7.36 (t, *J* = 9.0 Hz, 2H), 7.09–7.16 (m, 3H), 6.99–7.05 (m, 3H), 6.90 (t, *J* = 7.5 Hz, 1H), 6.63–6.70 (m, 3H), 6.49–6.55 (m, 5H), 5.98 (d, *J* = 8.0 Hz, 1H), 0.92 (s, 9H), 0.92 (s, 9H). MS: calcd *m/z* 1100.4 for [M]<sup>+</sup> (C<sub>59</sub>H<sub>49</sub>F<sub>2</sub>IrN<sub>8</sub>), found *m/z* 1100.3. Anal. Calcd for C<sub>59</sub>H<sub>49</sub>F<sub>2</sub>IrN<sub>8</sub>: C, 64.40; H, 4.49; N, 10.18. Found: C, 64.47; H, 4.54; N, 10.25.

**2.3.5. Synthesis of Complex 5.** The product was obtained by silica gel column chromatography with 1/4 (v/v) ethyl acetate/dichloromethane and then 1/1 (v/v) ethyl acetate/dichloromethane as eluent to give complex 5 (0.22 g) in a yield of 70%. <sup>1</sup>H NMR (500 MHz, CDCl<sub>3</sub>, δ [ppm]): 8.28 (d, *J* = 7.5 Hz, 1H), 7.91 (d, *J* = 5.5 Hz, 1H), 7.84 (t, *J* = 7.5 Hz, 1H), 7.56–7.70 (m, 8H), 7.38 (d, *J* = 7.5 Hz, 1H), 7.34 (d, *J* = 8.0 Hz, 1H), 7.12–7.20 (m, 4H), 7.05 (d, *J* = 8.0 Hz, 1H), 7.00 (d, *J* = 8.0 Hz, 1H), 6.96 (t, *J* = 7.5 Hz, 1H), 6.66–6.68 (m, 1H), 6.47–6.58 (m, 6H), 6.06 (d, *J* = 8.0 Hz, 1H), 0.92 (s, 9H), 0.87 (s, 9H). MS: calcd *m/z* 1154.3 for [M]<sup>+</sup> (C<sub>59</sub>H<sub>46</sub>F<sub>3</sub>IrN<sub>8</sub>), found *m/z* 1154.3. Anal. Calcd for C<sub>59</sub>H<sub>46</sub>F<sub>3</sub>IrN<sub>8</sub>: C, 61.39; H, 4.02; N, 9.71. Found: C, 61.42; H, 3.93; N, 9.77.

**2.4. Theoretical Calculations.** The density functional theory (DFT) calculations on electronic states of complexes 1–5 were obtained by B3LYP methods.<sup>16</sup> A double- $\xi$  quality basis set containing LANL2DZ was employed for Ir atoms, while a 6-31G\* basis set was used for other atoms. Solvent effects play a crucial role in predicting the absorption and PL spectra with time-dependent DFT (TD-DFT) calculations.<sup>17</sup> All calculations were obtained from the Gaussian 09 software package.<sup>18</sup>

**2.5. Electrochemical Measurements.** The reference electrode was an aqueous saturated calomel electrode, the working electrode was a glassy-carbon electrode, and the counter electrode was a platinum electrode. Cyclic voltammetric (CV) measurements were reported on a BAS 100 W instrument in CH<sub>2</sub>Cl<sub>2</sub> at a concentration of 10<sup>-3</sup> M. Ferrocene was used as the internal standard. The electrochemical data were obtained under nitrogen in CH<sub>2</sub>Cl<sub>2</sub>.

**2.6. Device Fabrication and Characterization.** Before they were loaded into a deposition chamber, glass substrates were cleaned ultrasonically with water, dried using an oven, and coated with indium tin oxide (ITO). Subsequently, various organic layers were deposited on the ITO-coated glass substrates by thermal evaporation. The active area of the device was set to 10 mm<sup>2</sup>, as defined by the shadow mask used for the cathode. The current density–voltage–luminescence (*J*–*V*–*L*) and current efficiency–luminescence–power efficiency ( $\eta_c$ –*L*– $\eta_p$ ) properties were obtained from both a programmable Keithley 2400 source meter and a Minolta LS-110 luminance meter.

**2.7. X-ray Crystallography.** The corresponding crystallographic data for complex 5 were collected on a Bruker Apex CCD II area-detector diffractometer. Absorption corrections were performed with multiscan techniques. The structure of complex 5 was refined by full-

matrix least squares with the SHELXL-97 program.<sup>19</sup> The non-hydrogen atoms were located by successive difference Fourier techniques. Hydrogen atoms were placed at calculated locations without further refinement of the parameters. Selected parameters of the molecular structure are given in Table S1 in the Supporting Information.

### 3. RESULTS AND DISCUSSION

**3.1. Single-Crystal Structure.** Figure 1 reports the X-ray structure of 5. For complex 5, the Ir(III) ion exhibits a

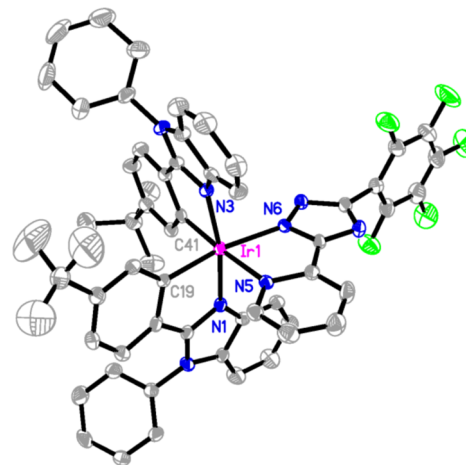


**Figure 1.** ORTEP drawing of complex 5. Thermal ellipsoids are drawn at 30% probability. The solvent molecules and hydrogen atoms are omitted for clarity.

distorted-octahedral geometry with cis-C,C and trans-N,N, as found for previously reported cyclometalated Ir(III) complexes.<sup>20</sup> The corresponding crystallographic characteristics and structure parameters are given in Table S1 in the Supporting Information. The associated Ir–N distances on the ancillary ligand (Ir1–N6 = 2.142(5) Å, Ir1–N5 = 2.136(6) Å) are significantly longer than those on the tbupbi ligand (Ir1–N1 = 2.049(5) Å, Ir1–N3 = 2.053(5) Å) because of the stronger electron-withdrawing abilities of triazole, confirming the anticipated  $\sigma$  donation of the carbons. In addition, owing to the steric hindrance of more fluorine atoms, the phenyl ring twists to the opposite position with respect to the triazole ring (N7–C53–C54–C55) with a value of 99.75°.

**3.2. Photophysical Properties.** Figure 2a depicts the absorption spectra of complexes 1–5 observed in CH<sub>2</sub>Cl<sub>2</sub> solution (10<sup>-5</sup> M) at room temperature. All complexes exhibit similar spectral features. The intense absorptions below 380 nm are the result of spin-allowed <sup>1</sup> $\pi$ – $\pi^*$  ligand-centered (<sup>1</sup>LC) transitions, whereas the weaker absorptions in the low-energy region (above 400 nm) can be attributed to <sup>1</sup>MLCT (metal-to-ligand charge transfer), <sup>1</sup>LLCT (ligand-to-ligand charge transfer), and <sup>3</sup>MLCT, <sup>3</sup>LLCT, <sup>3</sup>LC transitions.<sup>1b,21</sup> The strong spin–orbit coupling (SOC) endowed by the Ir(III) center partially allows the triplet emission, enabling the enhancement of phosphorescence efficiencies.<sup>21a</sup>

The PL spectra of 1–5 are shown in Figure 2b, and the relevant data are collected in Table 1. Almost identical spectral patterns with emission maxima at 498, 497, 495, 496, and 494 nm are observed at room temperature for 1–5, respectively. The measured lifetimes of the excited state are on the order of microseconds with values of 0.43, 0.50, 0.54, 0.45, and 0.59  $\mu$ s, respectively, which is the signature of phosphorescence for

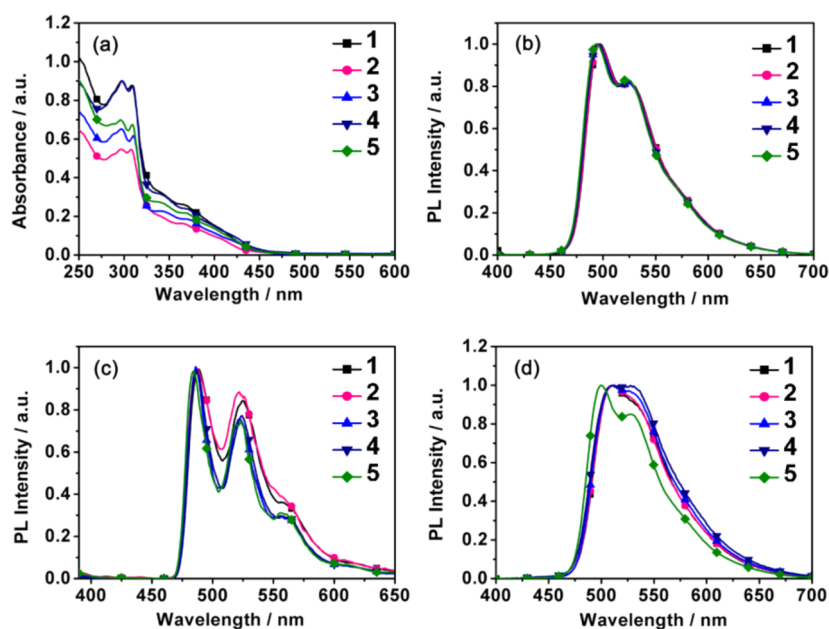


**Figure 2.** (a) UV-vis absorption spectra of complexes recorded in  $\text{CH}_2\text{Cl}_2$  solution. (b) PL spectra of Ir(III) complexes 1–5 at 298 K. (c) Low-temperature (at 77 K) PL spectra in  $\text{CH}_2\text{Cl}_2$  solution. (d) Neat film PL spectra of 1–5.

**Table 1. Photophysical Properties and Thermodynamic Stabilities of Complexes 1–5**

complex	$\lambda_{\text{PL,max}}^{a-c}$ (nm)	$\Phi_{\text{p}}$ (%)	$\tau^{a,c}$ ( $\mu\text{s}$ )	$E_{\text{g}}^d$ (eV)	$E_{\text{ox}}^e$ (V)	HOMO <sup>f</sup> (eV)	LUMO <sup>g</sup> (eV)	$T_{\text{d}}$ ( $^{\circ}\text{C}$ )
1	498, 488, 511	13	0.89, 0.43	2.23	0.41	−5.21	−2.98	407
2	497, 487, 511	20	0.89, 0.50	2.22	0.38	−5.18	−2.96	391
3	495, 486, 512	18	1.25, 0.54	2.22	0.38	−5.18	−2.96	422
4	496, 487, 511	14	1.14, 0.45	2.23	0.44	−5.24	−3.01	398
5	494, 484, 500	13	1.04, 0.59	2.22	0.47	−5.27	−3.05	394

<sup>a</sup>Measured in  $\text{CH}_2\text{Cl}_2$  solution at 298 K. <sup>b</sup>Measured in  $\text{CH}_2\text{Cl}_2$  solution at 77K. <sup>c</sup>Measured in spin-coated thin film. <sup>d</sup>Optical band gap. <sup>e</sup>Measured by CV using ferrocene as the internal standard. <sup>f</sup>Calculated from the onset oxidation potentials of the compounds. <sup>g</sup>Estimated by using the empirical equation  $E_{\text{LUMO}} = E_{\text{HOMO}} + E_{\text{g}}$ .

complexes 1–5.<sup>22</sup> As illustrated in Figure 2b, vibronic structures are clearly observed for complexes 1–5 at room temperature, indicating that their emissive excited states should contain the <sup>3</sup>LC excited state. Further comparison of the spectra at different temperatures shows that, in frozen glassy solvents at 77 K, the vibronic structure becomes better resolved and emission maxima exhibit apparent rigidochromism (9–10 nm) relative to those at room temperature (Figure 2c). In light of the shift in 77 K emission spectra, we speculate that both the <sup>3</sup>MLCT and <sup>3</sup>LLCT characters are also involved in the excited state of complexes 1–5.<sup>23</sup> On the basis of the above analysis, it is believed that their emission should originate from the admixture of <sup>3</sup>MLCT, <sup>3</sup>LLCT, and <sup>3</sup>LC characters.

Figure 2d displays the PL spectra in neat films of complexes 1–5, of which manifested obvious red shifts on going from the solutions to the neat films. This phenomenon may arise from molecular aggregation and triplet–triplet interaction in the solid state.<sup>24</sup> The PLQYs of complexes 1–5 were determined to be 13%, 20%, 18%, 14%, and 13%, respectively.

**3.3. Theoretical Calculations.** In order to understand the nature of the excited states of these phosphors, density functional theory (DFT) and time-dependent density functional theory (TD-DFT) calculations were carried out using B3LYP hybrid functional theory.<sup>16</sup> Figure 3 shows the energy levels and electron density distributions of the highest-occupied molecular orbitals (HOMO) and the lowest-unoccupied

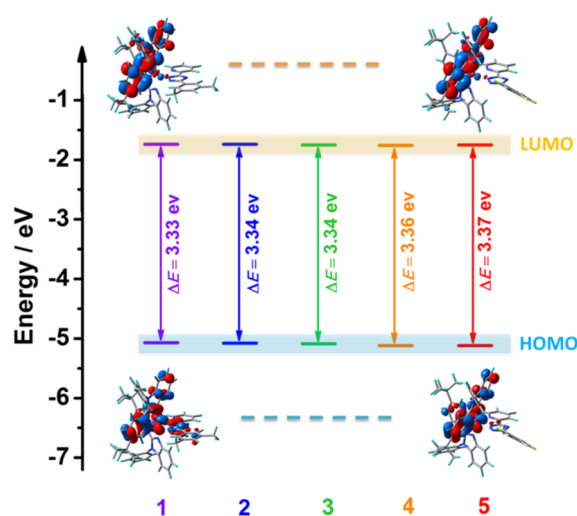


**Figure 3.** Electron distributions in HOMOs and LUMOs for complexes 1–5, together with the HOMO–LUMO band gaps.

molecular orbitals (LUMO) for complexes 1–5. Almost identical HOMOs and LUMOs with regard to the orbital character are obtained from the DFT calculations. For complex 1, the HOMO is comprised of Ir  $d\pi$  orbitals and the phenylbenzimidazole fragment of one main ligand, there being a small distribution from the ancillary ligand. The

LUMO resides on one of the cyclometalated ligands. According to the orbital distributions, the lowest triplet states ( $T_1$ ) of complex **1** originate from HOMO–LUMO (77%), possessing a mixture of  $^3\text{MLCT}$ ,  $^3\text{LLCT}$ , and  $^3\text{LC}$  transitions. These observations strongly indicate the existence of a rigidochromic shift and fine vibronic progression of the emission spectra at 77 K, consistent with the results of photophysical studies. Analogous conclusions are obtained for complexes **2**–**5**. In addition, theoretical calculations predict identical HOMO–LUMO energy gaps for complexes (3.33 eV for **1**, 3.34 eV for **2**, 3.34 eV for **3**, 3.36 eV for **4**, and 3.37 eV for **5**), further supporting their similar emission wavelengths in experiments.

**3.4. Electrochemical and Thermal Properties.** The electrochemical properties of complexes **1**–**5** were measured by cyclic voltammetry (CV). All of complexes exhibited irreversible oxidation process in  $\text{CH}_2\text{Cl}_2$  solution (Figure S6 in the Supporting Information). Their onset oxidation potentials are 0.41, 0.38, 0.38, 0.44, and 0.47 eV, respectively. The HOMO energy levels of complexes **1**–**5** were in the region of  $-5.18$  to  $-5.27$  eV. The LUMO levels were in the region of  $-2.96$  to  $-3.05$  eV, which were deduced from HOMO levels and optical band gaps.<sup>25</sup> As expected, complexes **1**–**5** have similar optical characteristics, and the electrochemical gaps found for **1** (2.23 eV), **2** (2.22 eV), **3** (2.22 eV), **4** (2.23 eV), and **5** (2.22 eV) are in accordance with the HOMO and LUMO energy gaps obtained from DFT calculations presented in the last section.

Thermal stabilities of complexes **1**–**5** were evaluated using TGA under nitrogen. From the TGA curves, **1**–**5** exhibit good thermal stability with decomposition temperatures ( $T_d$ ) as high as 407, 391, 422, 398, and 394 °C, respectively, which is desirable for the fabrication of state of the art OLEDs by a vacuum deposition approach. Notably, introducing fluorine substitutions has only a relatively small influence on the thermal stability, which is in good agreement with previous reports.<sup>12,26</sup>

**3.5. Electroluminescence Properties.** Doped OLEDs employing complexes **1**–**5**, namely A–E, were fabricated. The devices have a configuration as follows: ITO/MoO<sub>3</sub> (3 nm)/TAPC (35 nm)/TCTA (5 nm)/DCZppy:Ir (20%) (20 nm)/Bphen (40 nm)/LiF (0.5 nm)/Mg:Ag (120 nm, 15:1), in which MoO<sub>3</sub> and LiF serve as the hole-injecting layer (HIL) and electron-injecting layer (EIL). TAPC is 1,1-bis[4-[N,N'-bis(*p*-tolyl)amino]phenyl]cyclohexane, TCTA is 4,4',4''-tris(*N*-carbazolyl)triphenylamine, and Bphen is 4,7-diphenyl-1,10-phenanthroline. They act as the hole-transporting layer (HTL), electron blocking layer (EBL), and electron transporting layer (ETL), respectively. The energy level diagrams of the device and molecular structures of the compounds used are displayed in Figure 4. Complexes **1**–**5** were doped into DCZppy as the emitting layer, mainly due to the well-matched HOMO and LUMO energy levels of complexes **1**–**5** with that of DCZppy, enabling an efficient energy transfer from the host materials to the phosphor dopants. As far as we know, lower energy barrier between emitters and adjacent layers could make holes/electrons inject smoothly, which is helpful for optimizing the efficiency of devices. In this study, the HOMO/LUMO levels of TCTA are  $-5.7/2.3$  eV, which are all in the middle of those of TAPC ( $-5.6/2.0$  eV) and DCZppy ( $-6.05/2.56$  eV). Therefore, TCTA not only acts as a buffer gradient to facilitate hole injection but also blocks electron drift out of the host material, making holes and electrons effectively confined within the light-emitting layers and thus improving device performance.

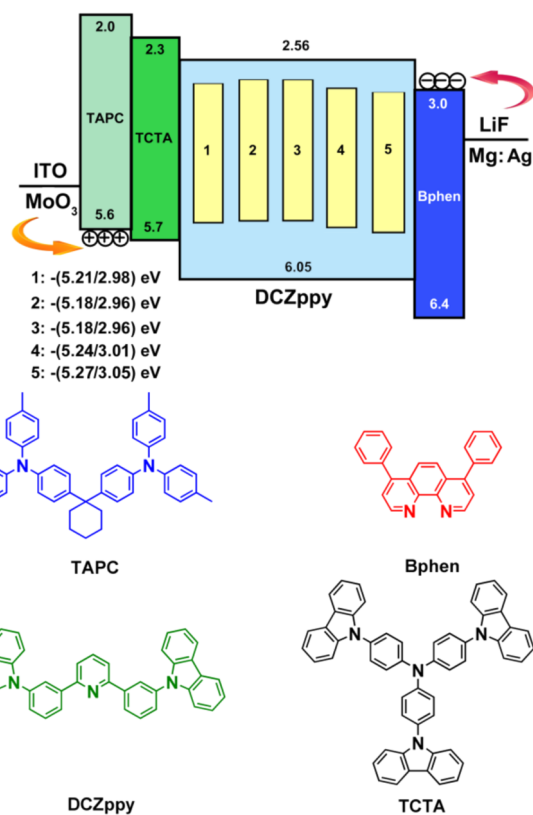


**Figure 4.** Energy levels and molecular structures of compounds used in devices.

The device configuration and other characteristics are shown in Figure 5. To fabricate the high doping concentration devices herein, the dopant concentration of devices A–E was kept at 20%. Figure 5b depicts the electroluminescence (EL) spectra of these devices with peaks centered at 502 nm for **1**, 502 nm for **2**, 501 nm for **3**, 498 nm for **4**, and 497 nm for **5**. Coincident with the data in the PL study, the EL spectral profile of each device is nearly identical with that of the PL counterparts, indicating the success in the OLED structure design for efficient energy transfer from the host material to the phosphors. In addition, this suggests that the emissions indeed originate from the triplet states of the phosphors regardless of the nature of the host materials.

Figure 5c,d describes current density–voltage–luminance ( $J$ – $V$ – $L$ ) characteristics and efficiencies versus luminance curves of devices A–E. The resulting devices emit bright green light at a low turn voltage of 3.0 V. Device A based on complex **1** without any fluorine atoms achieves a good current efficiency ( $\eta_c$ ) of 24.5  $\text{cd A}^{-1}$  and power efficiency ( $\eta_p$ ) of 19.3  $\text{lm W}^{-1}$ . Gratifyingly, device E employing complex **5** with five fluorine atoms as the emitting-layer exhibits much better EL performance with  $\eta_c = 32.6 \text{ cd A}^{-1}$  and  $\eta_p = 27.6 \text{ lm W}^{-1}$ , respectively. The results suggest that the modification of Ir(III) complexes using the appropriate number of fluorine groups can construct more efficient OLEDs to some extent. The strong intermolecular interactions occur in the host material and emitters, caused by the added fluorine atoms, facilitating energy transfer from the triplet of DCZppy to the Ir dopants. In addition, it is worth noting that all devices exhibit negligible drop-off with increasing brightness. For example, at the practical brightness of 1000  $\text{cd m}^{-2}$ , a small roll-off in luminance efficiency was observed and the power efficiency

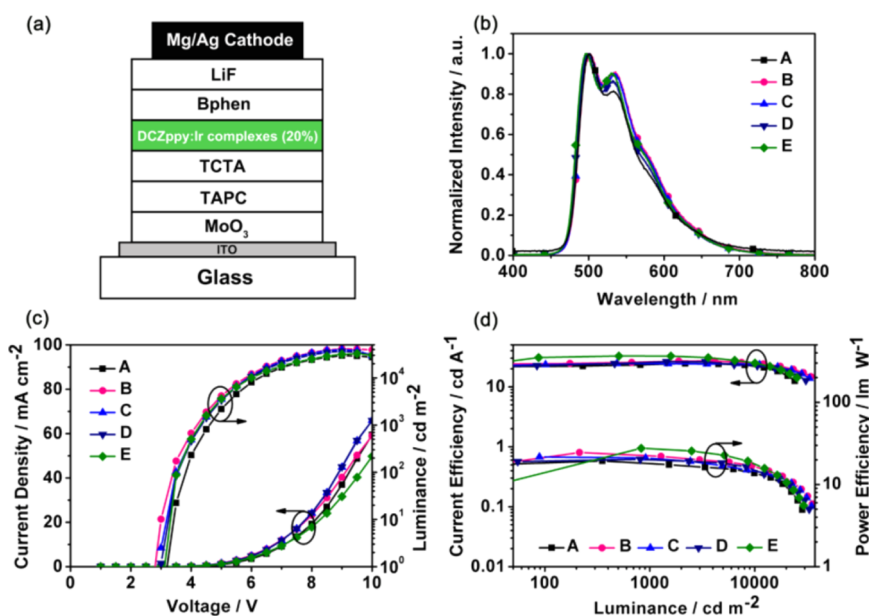


**Figure 5.** (a) Device configurations with doped EML at a concentration of 20%. (b) EL spectra of devices A–E. (c) Current density and luminance as a function of voltage for devices A–E. (d) Current efficiency and power efficiency versus luminance curves for devices A–E.

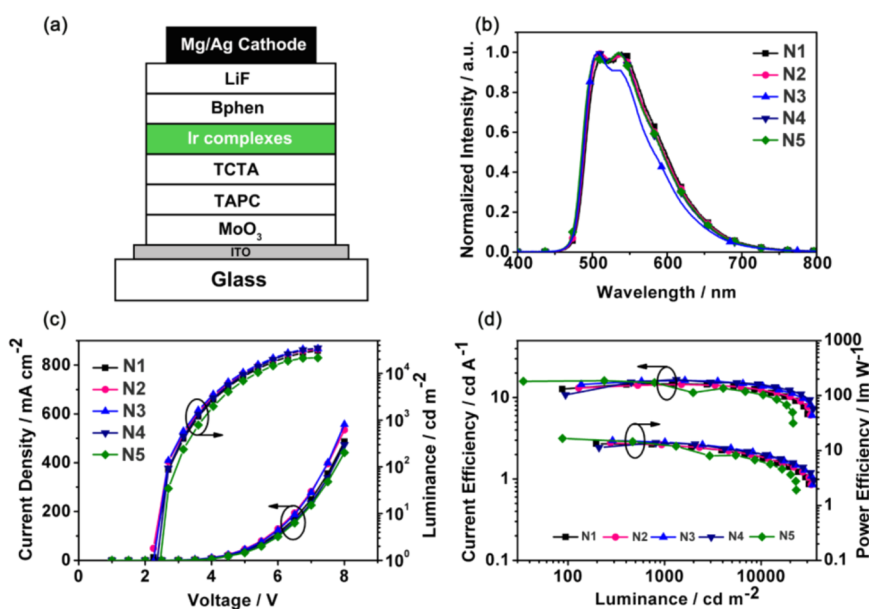


**Figure 6.** (a) Configuration of nondoped devices. (b) EL spectra of nondoped devices N1–N5. (c) Current density and luminance as a function of voltage for N1–N5. (d) Current efficiency and power efficiency versus luminance curves for devices N1–N5.

**Table 2. Summary of the EL Performance of Various Devices**

device	$V_{\text{turn-on}}^a$ (V)	$\lambda_{\text{EL}}$ (nm)	$\eta_c^{b,c}$ (cd A <sup>-1</sup> )	$\eta_p^{b,c}$ (lm W <sup>-1</sup> )	EQE <sup>b</sup> (%)	$L_{\text{max}}^b$ (cd m <sup>-2</sup> )	CIE ((x, y), V)
A	3.0	502	24.5, 23.5	19.3, 15.9	8.0	29610	(0.32,0.57), 5.0
B	3.0	502	26.8, 26.0	24.6, 19.3	8.6	41500	(0.32,0.57), 5.0
C	3.0	501	24.4, 24.3	21.6, 17.1	7.8	39900	(0.32,0.57), 5.0
D	3.0	498	26.2, 25.6	20.2, 18.3	8.6	36720	(0.31,0.56), 5.0
E	3.0	497	32.6, 32.6	27.6, 23.0	10.7	32710	(0.31,0.56), 5.0
N1	2.5	511	14.8, 14.7	13.3, 11.8	4.6	30390	(0.36,0.57), 5.0
N2	2.5	512	14.4, 14.3	13.7, 11.7	4.6	32540	(0.35,0.57), 5.0
N3	2.5	509	16.2, 16.1	15.2, 13.4	5.2	33670	(0.34,0.57), 5.0
N4	2.5	507	16.7, 16.3	13.9, 13.2	5.3	34680	(0.34,0.57), 5.0
N5	2.5	506	16.1, 14.2	16.6, 10.5	5.7	21450	(0.34,0.57), 5.0

<sup>a</sup>Voltages estimated at 1 cd m<sup>-2</sup>. <sup>b</sup>Maximum values of the various devices. <sup>c</sup>Measured at 1000 cd m<sup>-2</sup>.

of devices E still remains  $23.0 \text{ lm W}^{-1}$  without significant decay. If the excited-state characters of Ir(III) complexes are capable of being well controlled, introducing the fluorine substitutions in ancillary ligands favors the efficiency of doped OLEDs, in spite of a small effect on their photophysical and electrochemical behaviors and thermal stabilities. To the best of our knowledge, reports concerning devices with high efficiency and small roll-off value for high doping concentration attainable with phosphorescent Ir(III) complexes are relatively rare.

In order to further probe their nondoped EL properties, devices N1–N5 were fabricated with the multilayer configuration of ITO/MoO<sub>3</sub> (3 nm)/TAPC (35 nm)/TCTA (5 nm)/Ir (20 nm)/Bphen (40 nm)/LiF (0.5 nm)/Mg:Ag (120 nm, 15:1) (as depicted in Figure 6a). Figure 6b displays the EL spectra recorded at 5 V. Devices N1–N5 exhibit emissions at 506–512 nm, which resembled the PL spectra of these phosphors. Figure 6c shows the  $J$ – $V$ – $L$  characteristics for the nondoped devices N1–N5, and the relevant EL data are collected in Table 2. All of them display low turn-on voltages of 2.5 V and the maximum value of luminance ( $L_{\text{max}}$ ) reaches  $>20000 \text{ cd m}^{-2}$ . N5 shows a relatively lower  $L_{\text{max}}$  value in comparison to other nondoped devices. The phenomenon could be partially attributed to lower  $\Phi_p$  of the emitter. In addition, strong intermolecular interactions among the emitters caused by more fluorine atoms in the ligand may induce self-quenching effects, leading to inferior luminance.

The  $\eta_c$  and  $\eta_p$  versus luminance curves of devices N1–N5 are illustrated in Figure 6d. Devices N1 and N2 exhibit maximum  $\eta_c$  values of 14.8 and 14.4  $\text{cd A}^{-1}$  and  $\eta_p$  values of 13.3 and 13.7  $\text{lm W}^{-1}$ , respectively. In contrast, complexes 3–5 with fluorine atoms attached deliver superior device efficiencies. The  $\eta_c$  and  $\eta_p$  values of devices N3–N5 are in the range of 16.1–16.7  $\text{cd A}^{-1}$  and 13.9–16.6  $\text{lm W}^{-1}$ , respectively. It is noted that all nondoped devices except N5 exhibit little efficiency roll-off. For instance, the efficiencies are still as high as 16.1  $\text{cd A}^{-1}$  and 13.4  $\text{lm W}^{-1}$  for device N3 and 16.3  $\text{cd A}^{-1}$  and 13.2  $\text{lm W}^{-1}$  for device N4 at a brightness of 1000  $\text{cd m}^{-2}$ . The remarkable feature of the small efficiency roll-off may be due to the balanced charge transportation in these devices at high brightness.<sup>27</sup> Similar to the case for N3 and N4, device N5 based on complex 5 also reveals comparable efficiencies. Different from the doped device based on complex 5 as well as other nondoped counterparts, N5 shows relatively higher efficiency roll-off values. The phenomenon indicates that the greater number of fluorine atoms in the ligand may induce the strong intermolecular interactions among the emitters, leading to significant roll-off value at high luminance for the nondoped devices.<sup>12a,28</sup> That is to say, the ingenious modification of the number of fluorine atoms in the ancillary ligands will be an easy and feasible way to optimize EL devices possessing high performance and small efficiency roll-off.

#### 4. CONCLUSIONS

In summary, we designed and synthesized a class of new Ir(III) complexes 1–5, which have the same cyclometalated ligand and pyridyl-triazole derivatives as ancillary ligands modified with fluorine substituents. They were studied at a heavy doping level and as nondoped emitters in phosphorescent OLEDs. The heavy doping level devices exhibited promising performance with high efficiency and small roll-off; in particular for device E bearing five fluorine atoms,  $\eta_c = 32.6 \text{ cd A}^{-1}$  and  $\eta_p = 27.6 \text{ lm W}^{-1}$ , respectively. In terms of the nondoped devices, the combination of more fluorine atoms in the ancillary ligands

showed relatively higher efficiency roll-off, though achieving decent performances. The results suggest that rational incorporation of fluorine atoms in tuning the properties of materials can significantly improve device performances possessing high efficiency and small roll-off.

#### ■ ASSOCIATED CONTENT

##### Supporting Information

The Supporting Information is available free of charge on the ACS Publications website at DOI: 10.1021/acs.organomet.6b00753.

Supplemental schemes, figures, and X-ray structure data for complex 5 (PDF)

Crystallographic data for 5 (CIF)

Calculated structures (MOL)

#### ■ AUTHOR INFORMATION

##### Corresponding Authors

\*G.-G.S.: fax, +86-431-85684009; tel, +86-431-85099108; e-mail, shanggl187@nenu.edu.cn.

\*W.-F.X.: tel, +86-13844907598; e-mail, xiewf@jlu.edu.cn.

\*Z.-M.S.: e-mail, zmsu@nenu.edu.cn.

##### ORCID

Zhong-Min Su: 0000-0002-3342-1966

##### Notes

The authors declare no competing financial interest.

#### ■ ACKNOWLEDGMENTS

The authors gratefully acknowledge financial support from the National Natural Science Foundation of China (21303012, 21273030, 51203017, 21131001, and 60937001), 973 Program (2013CB834801), and the Science and Technology Development Planning of Jilin Province (20130204025GX).

#### ■ REFERENCES

- (1) (a) Forrest, S. R.; O'Brien, D. F.; You, Y.; Shoustikov, A.; Sibley, S.; Thompson, M. E. *Nature* **1998**, *395*, 151–154. (b) Lo, S. C.; Harding, R. E.; Shipley, C. P.; Stevenson, S. G.; Burn, P. L.; Samuel, I. D. W. *J. Am. Chem. Soc.* **2009**, *131*, 16681–16688.
- (2) D'Andrade, B. W.; Forrest, S. R. *Adv. Mater.* **2004**, *16*, 1585–1595.
- (3) (a) Thompson, M. E.; Djurovich, P. E.; Barlow, S.; Marder, S. *Comprehensive Organometallic Chemistry III*; Elsevier: Amsterdam, 2007; Vol. 12, pp 101–194. (b) Ding, J.; Wang, B.; Yue, Z.; Yao, B.; Xie, Z.; Cheng, Y.; Wang, L.; Jing, X.; Wang, F. *Angew. Chem., Int. Ed.* **2009**, *48*, 6664–6666. (c) You, Y.; Nam, W. *Chem. Soc. Rev.* **2012**, *41*, 7061–7084. (d) Hsieh, C. H.; Wu, F. I.; Fan, C. H.; Huang, M. J.; Lu, K. Y.; Chou, P. Y.; Yang, Y. H. O.; Wu, S. H.; Chen, I. C.; Chou, S. H.; Wong, K. T.; Cheng, C. H. *Chem. - Eur. J.* **2011**, *17*, 9180–9187. (e) Shan, G. G.; Li, H. B.; Sun, H. Z.; Zhu, D. X.; Cao, H. T.; Su, Z. M. *J. Mater. Chem. C* **2013**, *1*, 1440–1449. (f) Cao, H. T.; Shan, G. G.; Yin, Y. M.; Sun, H. Z.; Wu, Y.; Xie, W. F.; Su, Z. M. *Dyes Pigm.* **2015**, *112*, 8–16.
- (4) Haldi, A.; Kimyonok, A.; Domercq, B.; Hayden, L. E.; Jones, S. C.; Marder, S. R.; Weck, M.; Kippelen, B. *Adv. Funct. Mater.* **2008**, *18*, 3056–3062.
- (5) (a) Holder, E.; Langeveld, B. M. W.; Schubert, U. S. *Adv. Mater.* **2005**, *17*, 1109–1121. (b) Wong, W. Y.; Ho, C. L.; Gao, Z. Q.; Mi, B. X.; Chen, C. H.; Cheah, K. W.; Lin, Z. *Angew. Chem., Int. Ed.* **2006**, *45*, 7800–7803. (c) Zhang, Y.; Lai, S. L.; Tong, Q. X.; Lo, M. F.; Ng, T. W.; Chan, M. Y.; Wen, Z. C.; He, J.; Jeff, K. S.; Tang, X. L.; Liu, W. M.; Ko, C. C.; Wang, P. F.; Lee, C. S. *Chem. Mater.* **2012**, *24*, 61–70.
- (6) (a) Adamovich, V. I.; Cordero, S. R.; Djurovich, P. I.; Tamayo, A.; Thompson, M. E.; D'Andrade, B. W.; Forrest, S. R. *Org. Electron.*

- 2003, 4, 77–87. (b) Goushi, K.; Kwong, R.; Brown, J. J.; Sasabe, H.; Adachi, C. *J. Appl. Phys.* **2004**, 95, 7798–7802. (c) Peng, T.; Li, G.; Ye, K.; Wang, C.; Zhao, S.; Liu, Y.; Hou, Z.; Wang, Y. *J. Mater. Chem. C* **2013**, 1, 2920–2926.
- (7) Xu, H.; Chen, R.; Sun, Q.; Lai, W.; Su, Q.; Huang, W.; Liu, X. *Chem. Soc. Rev.* **2014**, 43, 3259–3302.
- (8) Liu, Y.; Ye, K.; Fan, Y.; Song, W.; Wang, Y.; Hou, Z. *Chem. Commun.* **2009**, 3699–3701.
- (9) (a) Holmes, R. J.; D'Andrade, B. W.; Forrest, S. R.; Ren, X.; Li, J.; Thompson, M. E. *Appl. Phys. Lett.* **2003**, 83, 3818–3820. (b) Wang, Y.; Herron, N.; Grushin, V. V.; LeCloux, D.; Petrov, V. *Appl. Phys. Lett.* **2001**, 79, 449–451. (c) Xie, H. Z.; Liu, M. W.; Wang, O. Y.; Zhang, X. H.; Lee, C. S.; Hung, L. S.; Lee, S. T.; Teng, P. F.; Kwong, H. L.; Zheng, H.; Che, C. M. *Adv. Mater.* **2001**, 13, 1245–1248.
- (10) Wu, W. C.; Yeh, H. C.; Chan, L. H.; Chen, C. T. *Adv. Mater.* **2002**, 14, 1072–1075.
- (11) (a) Cao, H.; Shan, G.; Wen, X.; Sun, H.; Su, Z.; Zhong, R.; Xie, W.; Li, P.; Zhu, D. *J. Mater. Chem. C* **2013**, 1, 7371–7379. (b) Cao, H.; Sun, H.; Yin, Y.; Wen, X.; Shan, G.; Su, Z.; Zhong, R.; Xie, W.; Li, P.; Zhu, D. *J. Mater. Chem. C* **2014**, 2, 2150–2159.
- (12) (a) Tordera, D.; Serrano-Pérez, J. J.; Pertegás, A.; Ortí, E.; Bolink, H. J.; Baranoff, E.; Nazeeruddin, M. K.; Frey, J. *Chem. Mater.* **2013**, 25, 3391–3397. (b) Chang, C. H.; Wu, Z. J.; Chiu, C. H.; Liang, Y. H.; Tsai, Y. S.; Liao, J. L.; Chi, Y.; Hsieh, H. Y.; Kuo, T. Y.; Lee, G. H.; Pan, H. A.; Chou, P. T.; Lin, J. S.; Tseng, M. R. *ACS Appl. Mater. Interfaces* **2013**, 5, 7341–7351. (c) Kozhevnikov, V. N.; Dahms, K.; Bryce, M. R. *J. Org. Chem.* **2011**, 76, 5143–5148. (d) Lee, J.; Oh, H.; Kim, J.; Park, K. M.; Yook, K. S.; Lee, J. Y.; Kang, Y. *J. Mater. Chem. C* **2014**, 2, 6040–6047. (e) Oh, H.; Park, K. M.; Hwang, H.; Oh, S.; Lee, J. H.; Lu, J. S.; Wang, S.; Kang, Y. *Organometallics* **2013**, 32, 6427–6436.
- (13) (a) Liu, C.; Mao, L.; Jia, H.; Liao, Z.; Wang, H.; Mi, B.; Gao, Z. *Sci. China: Chem.* **2015**, 58, 640–649. (b) Li, H. Y.; Li, T. Y.; Teng, M. Y.; Xu, Q. L.; Zhang, S.; Jin, Y. M.; Liu, X.; Zheng, Y. X.; Zuo, J. L. *J. Mater. Chem. C* **2014**, 2, 1116–1124.
- (14) (a) Shan, G. G.; Li, H. B.; Cao, H. T.; Zhu, D. X.; Li, P.; Su, Z. M.; Liao, Y. *Chem. Commun.* **2012**, 48, 2000–2002. (b) Wu, Y.; Sun, H. Z.; Cao, H. T.; Li, H. B.; Shan, G. G.; Duan, Y. A.; Geng, Y.; Su, Z. M.; Liao, Y. *Chem. Commun.* **2014**, 50, 10986–10989.
- (15) Orselli, E.; Kottas, G. S.; Konradsson, A. E.; Coppo, P.; Frohlich, R.; De Cola, L.; Van Dijken, A.; Buchel, M.; Borner, H. *Inorg. Chem.* **2007**, 46, 11082–11093.
- (16) Adamo, C.; Barone, V. *J. Chem. Phys.* **1999**, 110, 6158–6170.
- (17) Peach, M. J.; Williamson, M. J.; Tozer, D. J. *J. Chem. Theory Comput.* **2011**, 7, 3578–3585.
- (18) Frisch, M. J.; Trucks, G. W.; Schlegel, H. B.; Scuseria, G. E.; Robb, M. A.; Cheeseman, J. R.; Scalmani, G.; Barone, V.; Mennucci, B.; Petersson, G. A.; Nakatsuji, H.; Caricato, M.; Li, X.; Hratchian, H. P.; Izmaylov, A. F.; Bloino, J.; Zheng, G.; Sonnenberg, J. L.; Hada, M.; Ehara, M.; Toyota, K.; Fukuda, R.; Hasegawa, J.; Ishida, M.; Nakajima, T.; Honda, Y.; Kitao, O.; Nakai, H.; Vreven, T.; Montgomery, J. A., Jr.; Peralta, J. E.; Ogliaro, F.; Bearpark, M.; Heyd, J. J.; Brothers, E.; Kudin, K. N.; Staroverov, V. N.; Keith, T.; Kobayashi, R.; Normand, J.; Raghavachari, K.; Rendell, A.; Burant, J. C.; Iyengar, S. S.; Tomasi, J.; Cossi, M.; Rega, N.; Millam, J. M.; Klene, M.; Knox, J. E.; Cross, J. B.; Bakken, V.; Adamo, C.; Jaramillo, J.; Gomperts, R.; Stratmann, R. E.; Yazyev, O.; Austin, A. J.; Cammi, R.; Pomelli, C.; Ochterski, J. W.; Martin, R. L.; Morokuma, K.; Zakrzewski, V. G.; Voth, G. A.; Salvador, P.; Dannenberg, J. J.; Dapprich, S.; Daniels, A. D.; Farkas, O.; Foresman, J. B.; Ortiz, J. V.; Cioslowski, J.; Fox, D. J. *Gaussian 09, Revision D.01*; Gaussian, Inc., Wallingford, CT, 2013.
- (19) Sheldrick, G. M. *SHELXL-97*; Universität Göttingen, Göttingen, Germany, 1997.
- (20) (a) Huang, W. S.; Lin, J. T.; Chien, C. H.; Tao, Y. T.; Sun, S. S.; Wen, Y. S. *Chem. Mater.* **2004**, 16, 2480–2488. (b) Fernandez-Hernandez, J. M.; Beltran, J. I.; Lemaun, V.; Galvez-Lopez, M. D.; Chien, C. H.; Polo, F.; Orselli, E.; Frohlich, R.; Cornil, J.; De Cola, L. *Inorg. Chem.* **2013**, 52, 1812–1824.
- (21) (a) Nazeeruddin, M. K.; Humphry-Baker, R.; Berner, D.; Rivier, S.; Zuppiroli, L.; Graetzel, M. *J. Am. Chem. Soc.* **2003**, 125, 8790–8797. (b) Lamansky, S.; Djurovich, P.; Murphy, D.; Abdel-Razzaq, F.; Lee, H. E.; Adachi, C.; Burrows, P. E.; Forrest, S. R.; Thompson, M. E. *J. Am. Chem. Soc.* **2001**, 123, 4304–4312. (c) Xu, Q. L.; Liang, X.; Zhang, S.; Jing, Y. M.; Liu, X.; Lu, G. Z.; Zheng, Y. X.; Zuo, J. L. *J. Mater. Chem. C* **2015**, 3, 3694–3701.
- (22) (a) Costa, R. D.; Cespedes-Guirao, F. J.; Orti, E.; Bolink, H. J.; Gierschner, J.; Fernandez-Lazaro, F.; Sastre-Santos, A. *Chem. Commun.* **2009**, 3886–3888. (b) Su, H. C.; Fang, F. C.; Hwu, T. Y.; Hsieh, H. H.; Chen, H. F.; Lee, G. H.; Peng, S. M.; Wong, K. T.; Wu, C. C. *Adv. Funct. Mater.* **2007**, 17, 1019–1027.
- (23) (a) Li, J.; Djurovich, P. I.; Alleyne, B. D.; Yousufuddin, M.; Ho, N. N.; Thomas, J. C.; Peters, J. C.; Bau, R.; Thompson, M. E. *Inorg. Chem.* **2005**, 44, 1713–1727. (b) Wong, W. Y.; Ho, C. L. *J. Mater. Chem.* **2009**, 19, 4457–4482.
- (24) He, L.; Duan, L.; Qiao, J.; Wang, R.; Wei, P.; Wang, L.; Qiu, Y. *Adv. Funct. Mater.* **2008**, 18, 2123–2131.
- (25) Qin, T.; Ding, J.; Wang, L.; Baumgarten, M.; Zhou, G.; Müllen, K. *J. Am. Chem. Soc.* **2009**, 131, 14329–14336.
- (26) Kozhevnikov, V. N.; Zheng, Y.; Clough, M.; Al-Attar, H. A.; Griffiths, G. C.; Abdullah, K.; Raisys, S.; Jankus, V.; Bryce, M. R.; Monkman, A. P. *Chem. Mater.* **2013**, 25, 2352–2358.
- (27) (a) Jeon, S. O.; Yook, K. S.; Joo, C. W.; Lee, J. Y. *Appl. Phys. Lett.* **2009**, 94, 013301–013303. (b) Lee, J.; Lee, J. I.; Lee, J. Y.; Chu, H. Y. *Org. Electron.* **2009**, 10, 1529–1533. (c) Xu, Q. L.; Liang, X.; Jiang, L.; Zhao, Y.; Zheng, Y. X. *Dalton Trans.* **2016**, 45, 7366–7372.
- (28) (a) Sivasubramaniam, V.; Brodkorb, F.; Hanning, S.; Loebel, H. P.; Van Elsbergen, V.; Boerner, H.; Scherf, U. *J. Fluorine Chem.* **2009**, 130, 640–649.